JOURNAL OF MATERIALS SCIENCE 27 (1992) 5431–5440

Relationship between structure and mechanical properties for aramid fibres

R. J. YOUNG, D. LU, R. J. DAY
Polymer Science and Technology Group, Manchester Materials Science Centre, UMIST/University of Manchester, Manchester M60 1QD, UK

W. F. KNOFF
E.I. Du Pont De Nemours and Co. Inc., Spruance Research Laboratory, Richmond, VA 23261, USA

H. A. DAVIS
E.I. Du Pont de Nemours and Co. Inc., Textiles Department, Central Research, Wilmington, DE 19898, USA

The relationship between structure and mechanical properties for a series of twelve well-characterized aramid fibres has been determined. The fibres were produced under a variety of processing conditions and the fibre structure has been characterized using transmission electron microscopy. In particular, both the overall degree of molecular orientation in the fibres and the difference in structure between the fibre skin and core regions have been investigated in detail. The mechanical properties of the fibres have been evaluated using conventional mechanical testing and molecular deformation followed using Raman microscopy to monitor strain-induced band shifts. It has been shown that the mechanical properties of the fibres are controlled by the fibre structure. In particular, it is shown that the fibre modulus is governed by the overall degree of molecular orientation. It is also demonstrated that the fibre strength is controlled principally by the overall molecular orientation but may also be reduced by the presence of a highly-oriented skin region. It has been found that the rate of shift of the Raman bands per unit strain is proportional to the fibre modulus except for fibres with large differences in molecular orientation between fibre skin and core regions. For these fibres the rate of shift reflects the higher orientation of the skin.

1. Introduction

Over recent years one of the most exciting developments in polymer science has been in the area of high-performance fibres such as Kevlar®* aromatic polyamide (aramid) [1]. Such fibres exhibit high levels of stiffness and strength due to the high levels of molecular alignment achieved through the spinning of liquid crystalline solutions of inherently stiff molecules such as poly(*p*-phenylene terephthalamide) (PPTA) [1, 2]. There are now several different grades of aramid fibres available commercially which were produced by different routes and have different mechanical properties. Dobb and Robson [3] have recently examined structure/property relations for a series of commercial aramid fibres and have shown that the different mechanical properties reflect variations in fibre structure. In this present study on sets of experimental aramid fibres, a systematic variation in fibre structure has been examined. The relationship between the mechanical properties and structure of these fibres has been studied in detail and compared with that of commercially available fibres.

Molecular deformation in aramid fibres has also been followed using Raman microscopy. Previous studies have shown that the Raman bands in aramids shift to lower wave number on the application of strain [4, 5] indicating that mechanical deformation leads directly to molecular deformation in the fibres. Similar behaviour has been found for a wide variety of high-performance fibres such as gel-spun polyethylene [6], rigid rod polymer fibres [7–9], carbon fibres [10] and oriented polymer film [11]. It will be demonstrated that the use of Raman microscopy to study the deformation of aramid fibres allows a unique insight into the impact of skin/core structural differences upon fibre properties.

2. Experimental procedure

2.1. Materials

Twelve different types of aramid fibres were used in this present study and they are listed in Table I. There were four different groups of experimental fibres designated A, B, C and D. They were prepared with

* Du Pont Registered Trademark.

0022–2461

TABLE I Details of the microstructure of the different aramid fibres

Fibre	Diameter (μm)	2θ (degree)		$\langle \sin^2 \phi \rangle$	
		Skin	Core	Skin	Core
A1	10.3	11.5	13.7	0.0212	0.0301
A7	10.2	12.6	17.5	0.0255	0.0489
B1	15.8	13.8	14.9	0.0305	0.0355
B7	14.0	12.3	17.2	0.0243	0.0473
C1	18.7	12.8	13.0	0.0263	0.0271
C3	19.1	14.3	15.9	0.0328	0.0404
C5	18.4	15.9	16.9	0.0404	0.0456
C7	19.1	16.6	18.2	0.0441	0.0529
D1	12.8	12.1	12.8	0.0235	0.0263
E1	12.5	11.5	12.5	0.0212	0.0251
E2	11.9	11.9	12.9	0.0227	0.0267
F1	12.4	11.4	11.7	0.0209	0.0216

different diameters and the processing conditions were varied systematically in such a way as to produce either small differences in skin/core orientation ("1" type) or large differences in skin/core orientation ("7" type). None of the experimental A, B, C or D groups of fibres were heat treated. The properties of these experimental fibres were compared with the properties of three commercial-type fibres also listed in Table I. These consisted of two samples of Kevlar® 49 yarn (E1 and E2) and one of Kevlar® 149 (F1) which had all been heat treated.

2.2. Transmission electron microscopy

The fibres were prepared for transmission electron microscopy (TEM) by microtoming fibres embedded in a commercial "Spurr" epoxy resin. The resin block containing the fibres was cured at 70 °C for 8 h. It was then polished and trimmed with a freshly made glass knife into a trapezium shape with the fibre at the tip. The fibre was then microtomed longitudinally using a diamond knife with the direction of knife movement perpendicular to the fibre axis. Sections less than 100 nm thick were obtained from the central regions of the fibres. They were examined in a Philips 400T TEM operated at 120 kV. The beam intensity was kept at relatively low level to avoid beam damage. Selected-area diffraction patterns were obtained from different regions across the fibre section using a small (0.3 μm) selected-area aperture. The degree of molecular orientation in the diffraction patterns was measured using a Joyce–Loebl microdensitometer and each measurement reported is an average of at least five measurements from different diffraction patterns.

2.3. Mechanical testing

Young's modulus measurements were made by mounting individual aramid fibres on paper cards using a slow-setting epoxy resin cured at room temperature. The fibre diameters were measured using an Olympus Vanox optical microscope. Measurements were made at three different positions along the fibre axis and the average diameter was used to calculate the modulus of an individual fibre. The paper cards were then mounted on an Instron 1121 and after cutting the paper edges, stress–strain curves of the fibres were obtained using a crosshead speed of 2 mm min^{-1} and a load range of 1 N with a 5 N capacity load cell at 23 °C and 50% relative humidity (RH). For each gauge length (50, 90 and 130 mm, respectively) 20 specimens were employed, and the average modulus values were extrapolated to infinite gauge length to account for end effects.

The tensile strengths of the fibres were determined using individual fibres of 2 mm gauge length tabbed on paper. The small gauge length was employed to reduce the impact of strength variability along the fibre length and thus, obtain an accurate estimate of the true fibre strength [12]. They were strained at 20% min^{-1} at about 25 °C and 55% RH.

The sonic modulus of the fibres was measured on yarn using a prestress of the order of 0.1 g/den (about 10 MPa) and three measurements were made on each type of fibre.

2.4. Raman microscopy

Raman spectra were obtained from the aramid fibres during deformation in the Raman microprobe system. This is based upon a SPEX 1403 double monochromator connected to a modified Nikon optical microscope. Spectra were obtained using the 632.8 nm red line of a 7 mW He–Ne laser with an intensity of about 0.7 mW at the fibre. The spectra were collected using a highly sensitive Wright Instruments Charge-Coupled Device (CCD) camera cooled with liquid nitrogen. A $\times 40$ objective lens with a numerical aperture of 0.65 was used and this gave a 2 μm spot when focused [7–9]. The laser beam was polarized parallel to the fibre axis for all measurements.

Spectra were obtained from fibres during deformation in a small straining rig which fitted directly on the microscope stage. Individual fibres were fixed between aluminium foil tabs which were placed on to the aluminium blocks of the straining rig using cyanoacrylate adhesive, giving a gauge length of about 20 mm. This set-up allowed a precision of $\pm$ 0.05% for strain measurement [7–9]. Raman spectra were obtained during deformation by scanning the 1610 cm^{-1} Raman band of aramid fibres [4, 5] for small steps of strain of the order of 0.1%–0.2%.

3. Results and discussion

3.1. Transmission electron microscopy

The structure of the aramid fibres was studied in detail using transmission electron microscopy. The microtomed sections were examined in the electron microscope using low-dose techniques to avoid any potential radiation damage. Selected-area diffraction patterns (SADPs) were obtained from the skin and core regions of the sections. After each SAPD was obtained, a bright-field micrograph of the area was taken and the region in the selected-area aperture doubly exposed. In this way it was possible to follow differences in skin and core orientation for the various fibres.

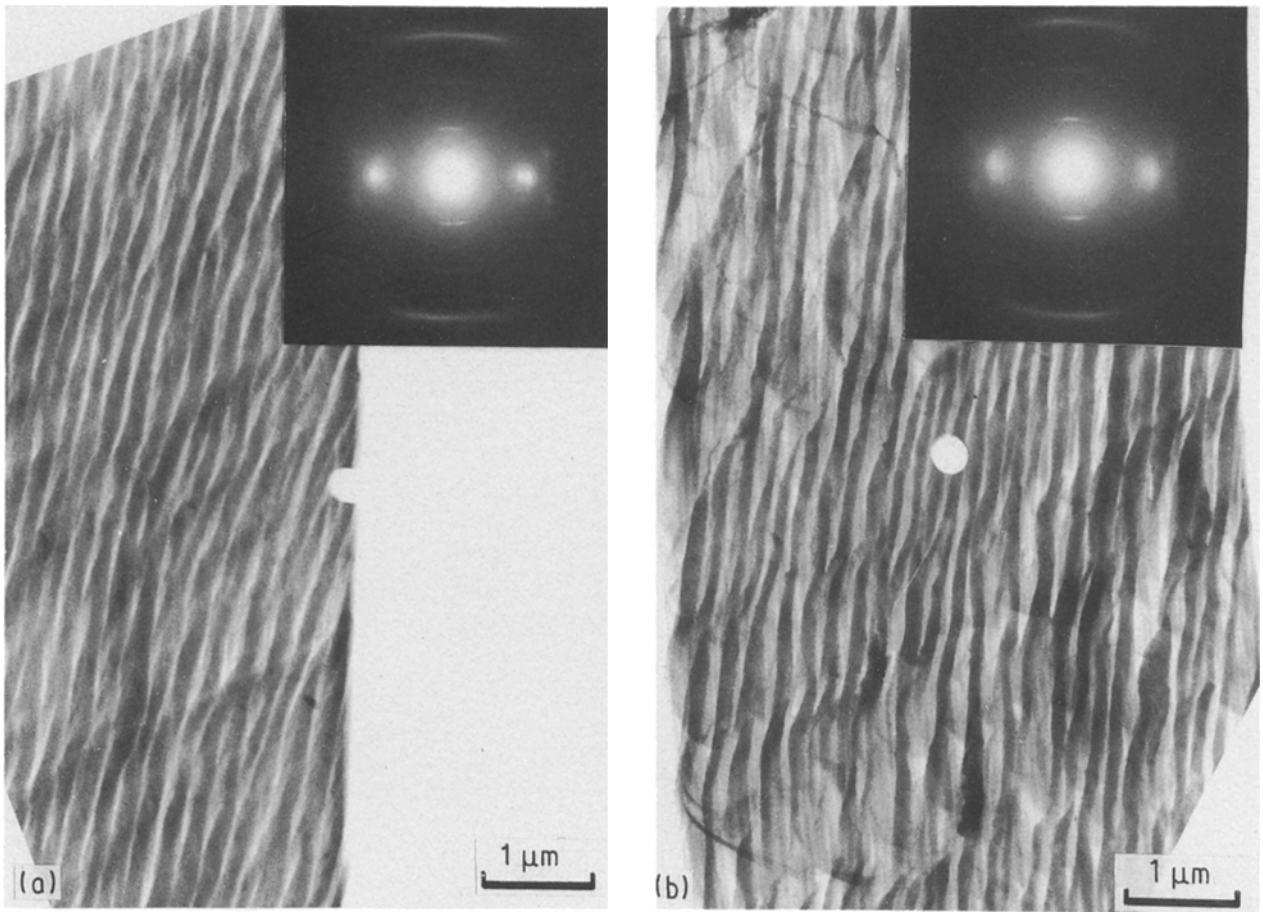

Figure 1 Transmission electron micrographs and selected-area electron diffraction patterns (inset) obtained from fibre B7. The doubly exposed region corresponds to the selected-area aperture. (a) Skin region, and (b) core region.

Fig. 1a and b show the micrographs and corresponding SADPs for the B7 fibre from the skin and core regions, respectively. It can be seen from examination of the spread of the arcs in the SAPDs that there is a much higher degree of orientation in the skin of the fibre (Fig. 1a) than in the core region (Fig. 1b). Very different behaviour is found for the F1 fibre as can be seen from Fig. 2. The SADPs obtained from skin (Fig. 2a) and core regions (Fig. 2b) both show a very high degree of molecular orientation.

Previous workers [3, 13–15] have noted that there may be a difference in structure between the skin and core regions in aramid fibres. Li *et al.* [13] investigated the structure of Kevlar® 49 fibres and demonstrated that the fibres exhibited a skin and core structure although they did not quantify the differences. Chatzi *et al.* [14] used an infrared photoacoustic technique to show differences in orientation of the polymer chains between the skin and core regions of Kevlar® 49 fibres. Yang *et al.* [15] found evidence for a skin/core structure during measurement of the strain birefringence of Kevlar® fibres subjected to static loading. Finally, Tiefenthaler and Urban [16] demonstrated a difference between skin and core structure in Kevlar® fibres using the relatively-new technique of Circle ATR FT–IR.

An attempt has been made in this present study to quantify the degree of molecular orientation in the fibres using a microdensitometer to measure the spread of the arcs in the diffraction patterns. The procedure is shown schematically in Fig. 3. The intensity is measured first along the equatorial line of the SADP. This then allows the position of the 1 1 0/2 0 0 peaks to be determined and the baseline in this region to be defined. A second scan is then made at 90° to the first scan across the 1 1 0/2 0 0 peak and the half-height width of this scan, 2θ, enables an estimate of the degree of molecular orientation to be obtained. It must be noted that this is only a semi-quantitative measure of the degree of orientation because the data have not been corrected for instrumental broadening, and do not take into account factors such as crystalline size or lattice distortion [3]. However, the measurements do enable a simple comparison of the levels of crystalline order between skin and core regions in the same fibre and between different fibres and it will be shown that the fibre properties can be related to these structural differences.

The values of 2θ measured for the skin and core regions of the twelve different fibres are presented in Table I along with measurements of average fibre diameter for each fibre. Each value of 2θ quoted is the mean of at least five different measurements for the individual fibres. It can be seen that the highest degree of orientation (i.e. lowest value of 2θ) is obtained for the F1 fibre and the poorest orientation is found for fibre C7. It is also significant that for all the fibres the level of molecular orientation is higher for the skin

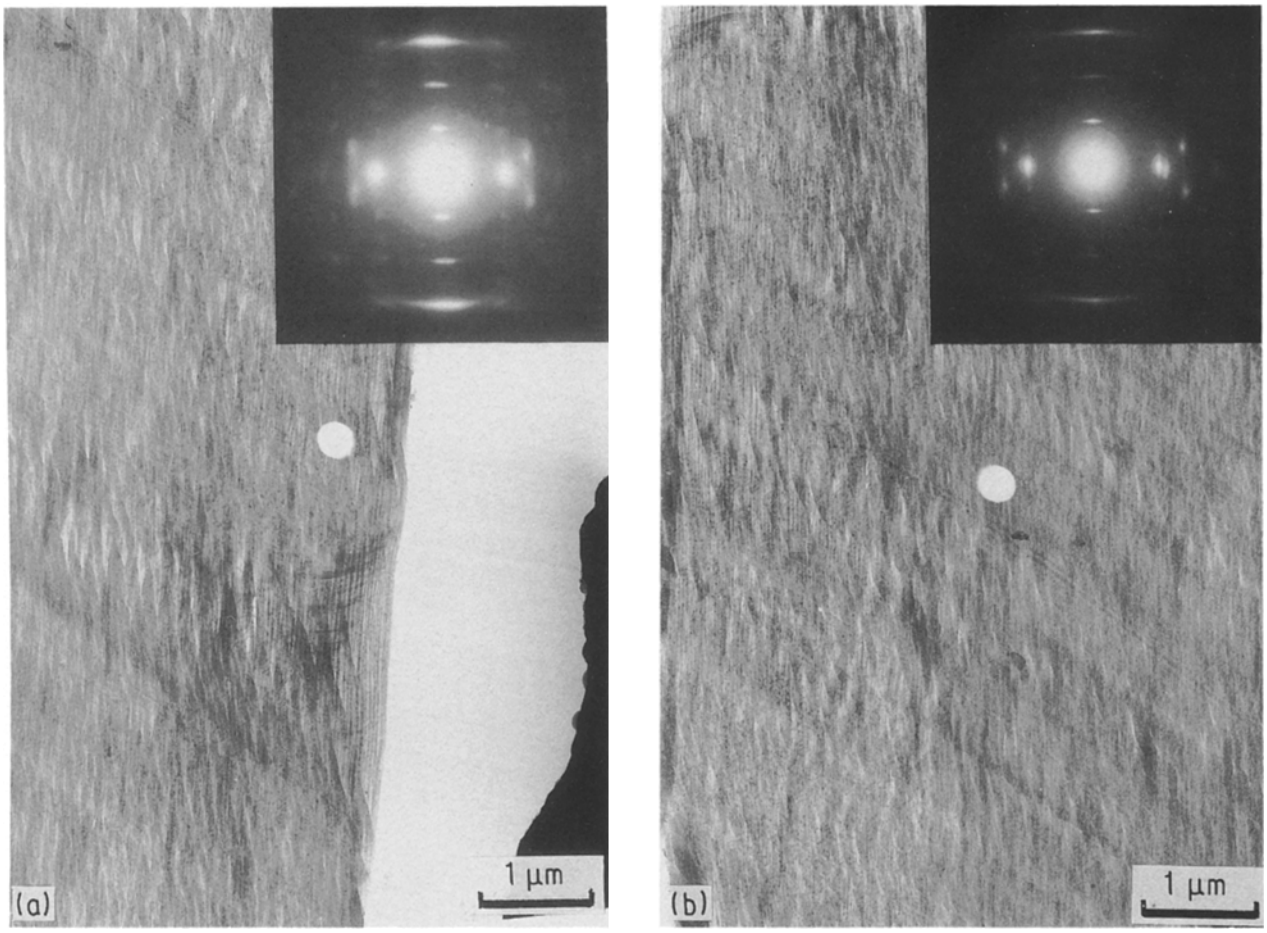

Figure 2 Transmission electron micrographs and selected-area electron diffraction patterns (inset) obtained from fibre F1. The doubly exposed region corresponds to the selected-area aperture. (a) Skin region, and (b) core region.

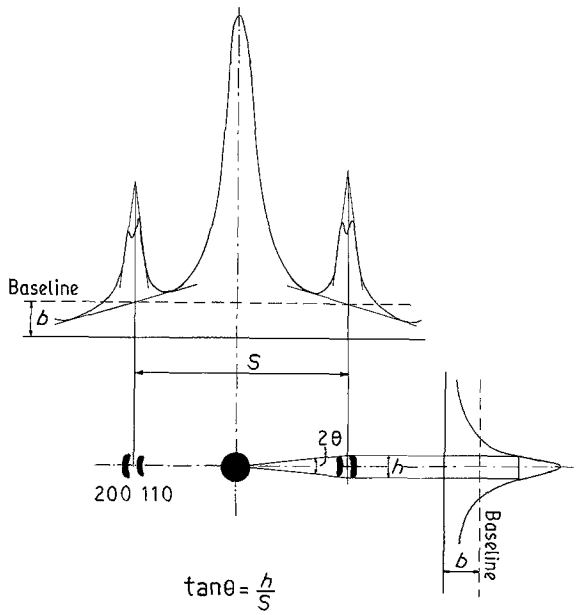

Figure 3 Schematic illustration of the method of determining the degree of molecular orientation from the electron diffraction patterns.

regions than for the fibre core regions and it should be noted that there is a particularly large difference in skin/core orientation for the A7 and B7 fibres ($\Delta 2\theta \approx 5°$).

Because the size of the selected-area aperture (≈ 0.3 μm) is significantly smaller than the diameter of the fibres it was possible to obtain an idea of the variation in orientation across the fibre cross-section by taking a series of SADPs in steps of about 1 μm across the fibre diameter. Care had to be taken to minimize radiation damage by keeping the dose of radiation at low levels and avoiding any unnecessary exposure of the fibres to the electron beam. Fig. 4a and b show the variation of 2θ with position across the fibre diameter for the F1 and A7 fibres, respectively. The scatter in the individual measurements of 2θ of about $\pm 0.5°$ can be seen from the plots. The variation of 2θ between the skin and core regions of the A7 fibre can be clearly seen and it should be noted that there is a gradual rather than step change in 2θ across the fibre diameter. Hence there is no sharp differentiation between the fibre skin and core for the A7 fibre. In contrast, there is little change in 2θ across the F1 fibre with only a slightly higher degree of orientation in the skin regions.

3.2. Mechanical testing

The mechanical testing data for the different fibres are given in Table II. It can be seen that the Young's modulus of the fibres varies between 67 GPa for the C7 fibres and 161 GPa for F1. The sonic modulus shows similar behaviour and reflects differences in

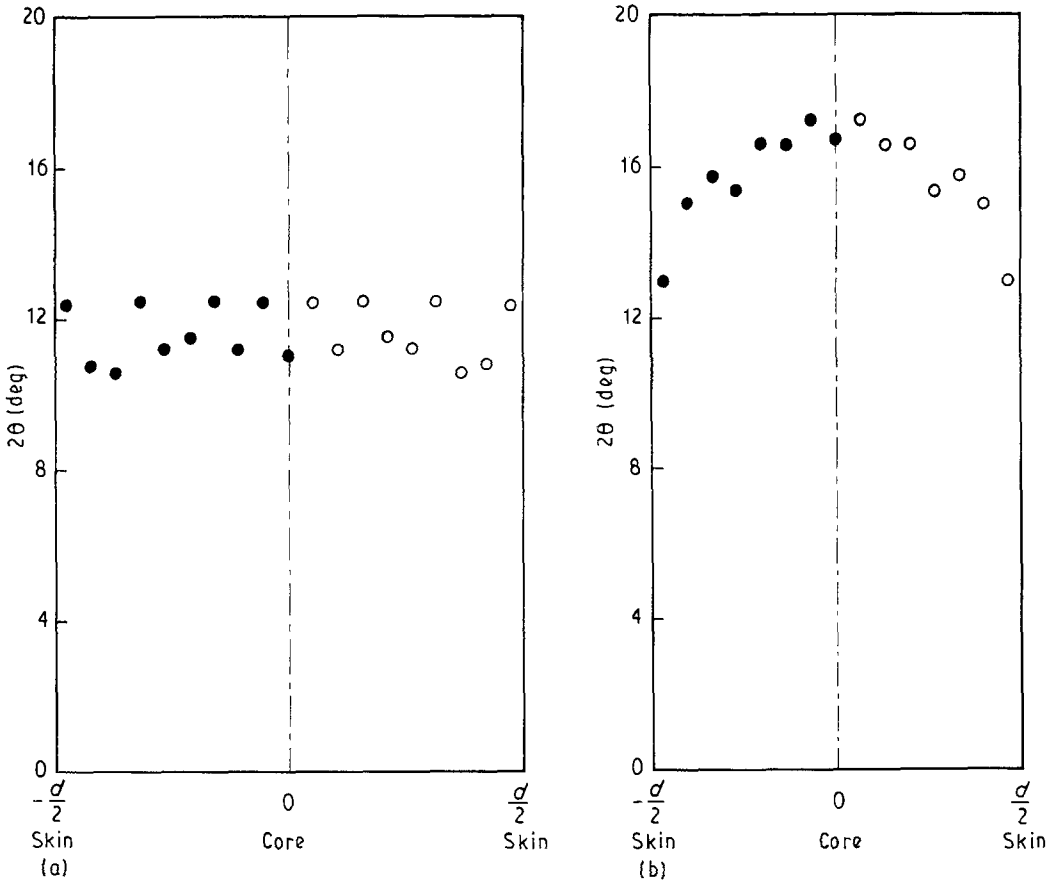

Figure 4 Variation in (●) the measured values of 2θ with position across the diameter of the fibres. (a) F1 and (b) A7. (○) The assumed mirror-image values of 2θ.

TABLE II Details of the mechanical properties of the aramid fibres

Fibre	Young's modulus (GPa)	Sonic modulus (GPa)	Fracture strength (GPa)	$d\Delta\nu/de$ (cm^{-1}/%)
A1	128	160	4.77	4.0
A7	94	111	3.27	4.0
B1	116	144	4.32	3.9
B7	90	112	3.09	3.6
C1	99	134	4.14	3.3
C3	79	112	3.07	2.8
C5	67	92	3.20	2.2
C7	67	98	3.05	2.1
D1	94	131	4.22	3.2
E1	124	–	4.20	4.0
E2	129	156	4.13	4.0
F1	161	143	3.30	5.2

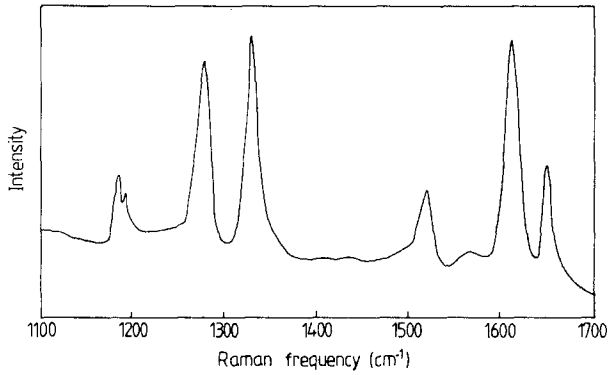

Figure 5 Raman spectrum for a single E1 fibre between 1100 and 1700 cm^{-1} obtained using a He–Ne laser.

molecular orientation in the fibres. There is also a wide range in fracture strength which increases from 3.05 GPa for fibre C7 to 4.77 GPa for fibre A1.

3.3. Raman microscopy

Well-defined Raman spectra could be obtained from the fibres as described earlier [4, 5]. Fig. 5 shows the Raman spectrum for an E1 fibre between 1100 and 1700 cm^{-1} showing six well-defined peaks. It was shown in an earlier publication [4] that the position of all six bands shifts to lower frequency under the application of stress or strain to the fibres. Examples of this are shown for the strong 1610 cm^{-1} phenylene-group stretching band in Fig. 6a and b. It can be seen that at a strain of level of 1% there is a measurable shift in the position of the band to lower frequency for both the C7 and F1 fibres. In addition it can be seen that the shift in band position is greater for the higher modulus (Table II) F1 fibre than for the lower modulus C7 fibre. The position of the peaks was determined by fitting a Gaussian curve to the data and Fig. 7a and b show the shift in peak position with strain for the two types of fibre. The data fall approximately on straight lines and it can be seen that the slope of the line $d\Delta\nu/de$ (where $\Delta\nu$ is the Raman frequency and e is the strain) is higher for the higher modulus F1 fibre than for C7. It should also be noted that the strain to failure is different for the two fibres in Fig. 7 with the C7 fibre showing significantly higher elongation at

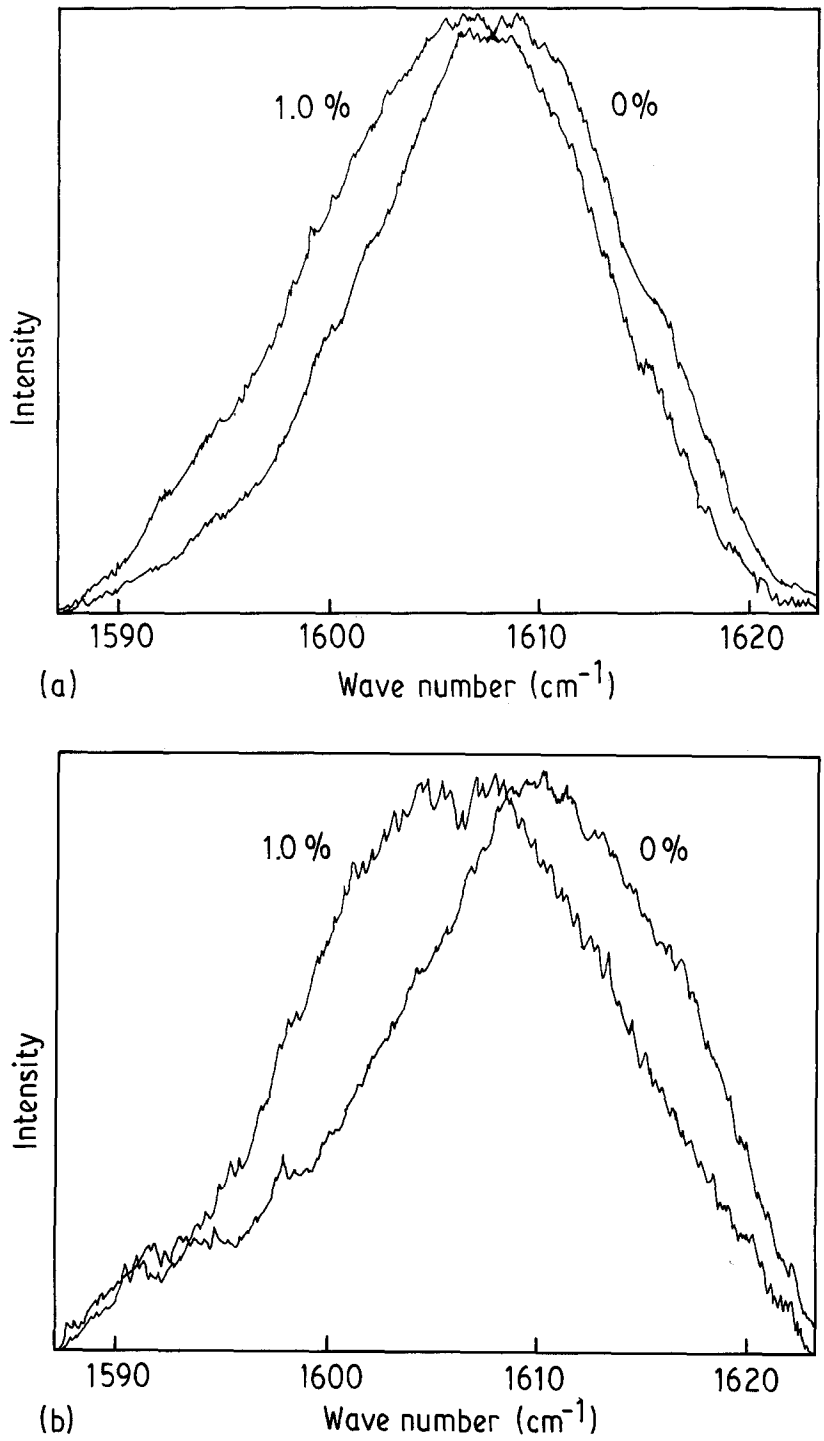

Figure 6 The peak position of the 1610 cm^{-1} Raman band unstrained and at a strain of 1% for fibres (a) C7, and (b) F1.

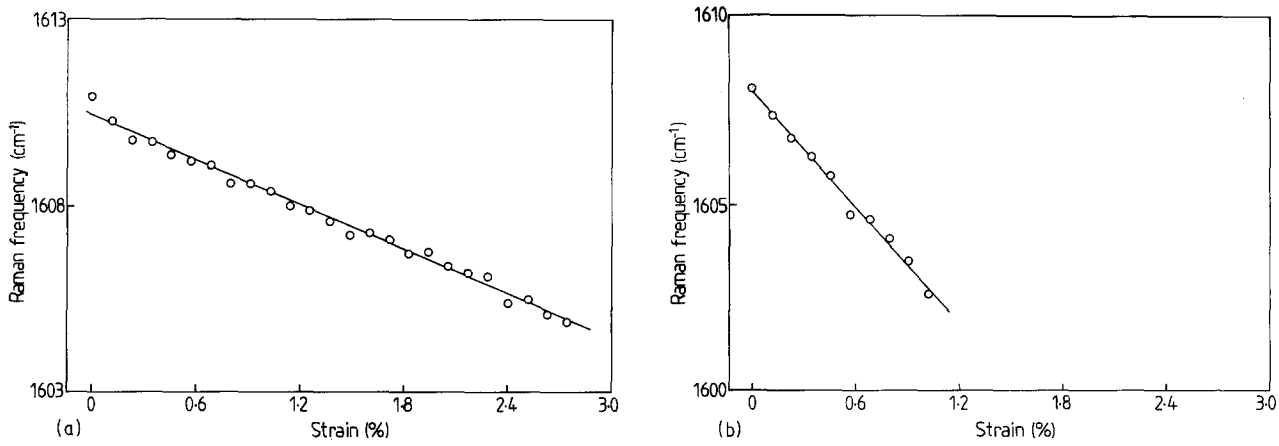

Figure 7 Dependence of the position of the 1610 cm^{-1} Raman band upon strain for fibres (a) C7, and (b) F1.

failure. The measured values of $d\Delta\nu/de$ for the twelve different fibres are also given in Table II.

4. Discussion

4.1. Fibre modulus

Comparing Tables I and II shows that there is a considerable variation in fibre modulus, E, with structure. In particular, it appears that E is controlled principally by the level of molecular orientation, 2θ, in the core regions. The highest modulus fibres tend to have the lowest core values of 2θ. The deformation of aromatic polyamide fibres has been modelled by Northolt and co-workers [17–19]. They considered the fibres to be made up of a series of end-to-end linked crystallites each having a slight disorientation with respect to the fibre axis. A tensile stress, σ, applied parallel to the fibre axis causes both stretching of the crystallites and a rotation towards the fibre axis due to shear deformation. The total strain is then the sum of the strain due to the two deformation processes,

$$e_{\text{total}} = e_{\text{stretch}} + e_{\text{rotation}} \quad (1)$$

or

$$e_{\text{total}} = \frac{\sigma}{E_c} + 0.5\langle\sin^2\phi\rangle[1 - \exp(-\sigma/g)] \quad (2)$$

where E_c is the PPTA crystal chain direction modulus, $\langle\sin^2\phi\rangle$ is an orientation parameter describing the average molecular orientation with respect to the fibre axis and g is the shear modulus in the chain direction. The orientation parameter is related to the Young's modulus, E, of the fibre through

$$\frac{1}{E} = \frac{1}{E_c} + \frac{\langle\sin^2\phi\rangle}{2g} \quad (3)$$

It has been shown [19] that the above equation can be used to model the stress–strain behaviour of aromatic polyamide fibres at small strains (< 2%), in particular the relationship between the measured fibre modulus and the degree of molecular orientation in the fibres. The theory of Northolt and co-workers has been recently developed and generalized by Allen and Roche [20] in order to account for the supramolecular structure of Kevlar®. However, their final equation is similar to Equation 2 except that the sine function is replaced by a tangent function. For small angles this will not lead to large differences between the two approaches.

It is known [18] that if the azimuthal profile of the 110/200 reflection can be fitted to a Lorentz-IV distribution, the orientation parameter $\langle\sin^2\phi\rangle$ is related to the half-height width, 2θ, approximately by

$$\langle\sin^2\phi\rangle = 2.114\sin^2\theta \quad (4)$$

This equation has been used to derive the values of $\langle\sin^2\phi\rangle$ listed in Table I for the different fibres. Northolt [18] showed that an equation of the form of Equation 3 could be used to explain the dependence of the sonic modulus, E_s, upon $\langle\sin^2\phi\rangle$ for a series of aromatic polyamide fibres. In particular, he demonstrated that $1/E_s$ was proportional to $\langle\sin^2\phi\rangle$ for three fibres deformed to different levels of strain.

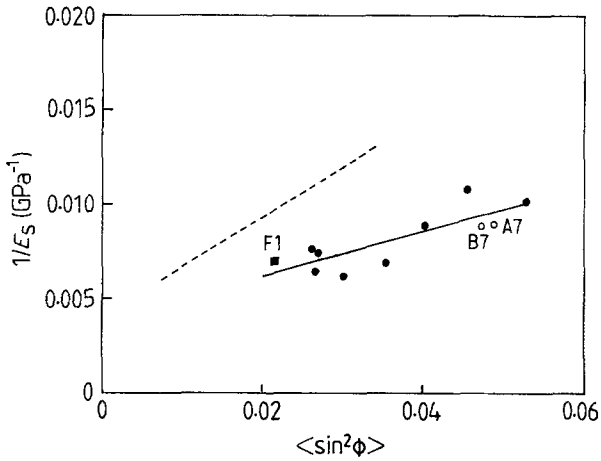

Figure 8 Variation of the reciprocal of the sonic modulus of the fibres $1/E_s$ with $\langle\sin^2\phi\rangle$. (– – –) X-ray data of Northolt [18].

A similar analysis has been performed in this present study as can be seen in Fig. 8 where the reciprocal of the sonic modulus (Table II) for each fibre is plotted against the core value of $\langle\sin^2\phi\rangle$ (Table I). The core values have been chosen because the core regions tend to have the most uniform structure and account for most of the fibre cross-sectional area (Fig. 4). It can be seen that the data fall approximately on a straight line with an intercept on the $1/E_s$ axis corresponding to an E_s value of about 260 GPa given by a linear regression analysis. Northolt's line [18] is also plotted in Fig. 8 and although the two lines have a different slope, the intercept is approximately the same ($E_s \approx 240$ GPa). It has been shown that this intercept corresponds to the situation when there is only crystal stretching and no rotation and so is essentially the crystal modulus, E_c, in the chain direction.

At this stage it is of interest to consider why the two lines in Fig. 8 are not in the same position. Firstly, the values of $\langle\sin^2\phi\rangle$ for the present fibres have been determined directly from the 2θ values measured from the electron diffraction patterns and have not been corrected for instrumental broadening and other factors. It is not clear if Northolt [18] had corrected his data for this effect but others [3] have corrected their X-ray data when characterizing the degree of orientation in aromatic polyamide fibres. Obviously, such corrections will have the effect of reducing the values of $\langle\sin^2\phi\rangle$ and so make the two lines in Fig. 8 closer. If the corrections are due to a systematic error then they will tend only to affect the slopes of the lines in Fig. 8 and not the intercepts. A second factor which will reduce $\langle\sin^2\phi\rangle$ for each fibre is the fact that only core values of $\langle\sin^2\phi\rangle$ have been used. Clearly, it would be desirable to have weighted values of $\langle\sin^2\phi\rangle$ which take into account the variation of 2θ with position across the fibre (cf. Fig. 4). However, because such distributions are very time consuming to obtain and were only available for two fibres, it was decided to use the core values of $\langle\sin^2\phi\rangle$ as a first approximation. Nevertheless, the similarity between the values of E_c found using the X-ray data and that obtained using

electron microscopy shown in Fig. 8 gives confidence in the present analysis.

Northolt and Sikkema [21] have recently reviewed the various attempts to calculate and measure the value of E_c for aromatic polyamide molecules. Direct measurement of crystal lattice strain along the fibre axis using X-ray diffraction [22] yields a value of 200 GPa, whereas Barton [23] found an E_c value of 218 GPa by extrapolation of the relationship between lattice distortion and the fibre modulus. Various theoretical estimates of the chain direction modulus have yielded values of 200 GPa [24], 182 GPa [25] and 204 GPa [26], respectively. It appears, therefore, that the analysis using Equation 3 (Fig. 8) yields a value of E_c which is somewhat higher than that found by other methods. This may be because the theory is not strictly correct or, more likely, due to difficulties in obtaining values of $\langle \sin^2 \phi \rangle$ free from error.

It is also possible to estimate a value of the shear modulus, g (from Equation 3), for the fibres from the slope of the solid line in Fig. 8. A value of g of 4.2 $\pm$ 0.9 GPa is obtained. This is significantly higher than previous estimates [19, 20, 27] which were of the order of 2 GPa. Again, this discrepancy is probably due to taking core values of $\langle \sin^2 \phi \rangle$ which were not corrected for instrumental broadening or other factors.

4.2. Fibre strength

With such a well-characterized set of aramid fibres, it is certainly worth considering the factors which may be influencing the fracture strength, σ_f. As has been mentioned previously, all the strength data (Table II) were from tests performed at 2 mm test length. Considerable work [12] has been done to determine and model the strength of Kevlar® fibres and the variation in strength along the length of the filaments. This has shown that the 2 mm test length is reasonable for obtaining a good estimate of the fibre strength free of the effects of random defects and periodic strength variations [12].

The results of many well-established theories regarding the tensile properties of solids [28], twisted yarns [29], and fibre-reinforced composites [30], lead to the expectation that in polymeric fibres both modulus and fracture strength should increase as orientation increases. The theoretical and observed relationships between modulus and the molecular orientation, as estimated by the electron diffraction experiments, have been discussed in the previous section. Thus, there are available three independent estimates of the average molecular orientation in these fibres; Young's modulus, sonic modulus and the electron diffraction data. If the F1 data pairs are set aside, the fracture strength correlates well with each of these orientation-sensitive properties (Fig. 9).

These data provide the added opportunity to explore the possible impact of skin/core orientation differences on the fracture strength of aramid fibres. This, however, must be done with the understanding that such an effect will likely be small and that the orientation estimates available (electron diffraction and modulus) are estimates of that in the unstressed fibre and not that of the fibre just prior to failure. The skin/core effect would be manifested in the scatter of the strength data about the linear regression relationship in Fig. 9 and, indeed, it can be seen that, in the strength versus Young's modulus plot (Fig. 9), the two samples with the highest skin/core delta (A7 and B7) lie significantly below the regression relationship. This lower-than-expected strength may be due to the added impact of the skin/core structure. The statistical significance of the skin/core delta has been further established by performing a simple multiple linear regression of the strength as a function of modulus and the skin/core 2θ delta. The 2θ delta property was found to be a significant variable with a 1° increase in the skin/core 2θ delta associated with an approximately 0.15 GPa decrease in fracture strength. The mechanism by which a mismatch in the structure and mechanical properties between the skin and core regions can have a deleterious effect upon the fibre strength is quite simple. The more highly oriented skin region of the fibre will have higher modulus and lower elongation to failure than the core. Therefore, under conditions of uniform strain, the skin will fail first and initiate the failure of the entire fibre. This phenomenon will be discussed further in the next section with respect to the Raman band shift data.

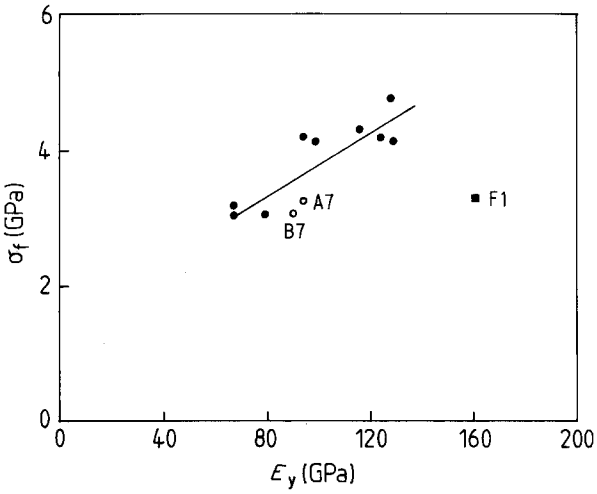

Figure 9 Dependence of the fibre strength, σ_f, upon the Young's modulus, E_y, for the fibres.

It is also of interest to consider why the F1 fibres have relatively low strength in view of their high value of Young's modulus, E_y. Smith and Termonia [31] have considered the factors which control the strength of Kevlar® fibres such as chain-end segregation. Dobb and Robson [3] have used transmission electron microscopy to examine the differences between F1 and other fibres. They reported the presence of defect layers in F1 fibres and suggested that such defects would lead to a significant reduction in fibre strength. Another factor leading to the lower tensile strength of the F1 fibres may be simply the low shear strength between the crystallites within the fibres.

4.3. Molecular deformation

It is known that Raman microscopy gives a unique insight into the mechanisms of molecular deformation

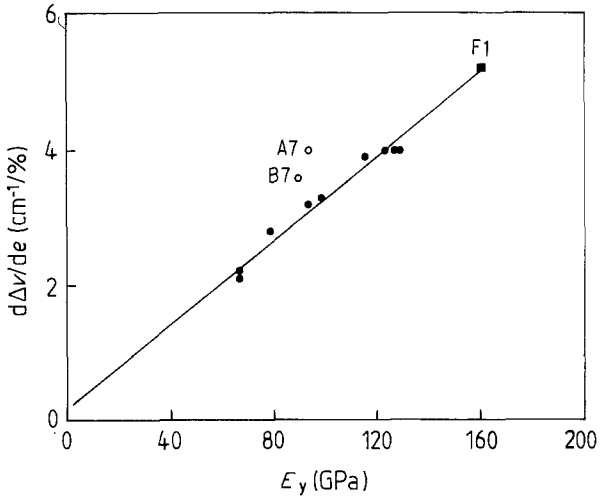

Figure 10 Variation of the strain sensitivity of the position of the 1610 cm^{-1} Raman band, $d\Delta\nu/de$, with Young's modulus, E_y, for the different aramid fibres.

in high-performance polymer fibres [4–9]. The results in Figs 6 and 7 and in Table II show clearly that the macroscopic deformation of aramids is translated directly into molecular deformation. Inspection of the data in Table II shows that there is a general increase in $d\Delta\nu/de$ with fibre modulus. Fig. 10 shows a plot of $d\Delta\nu/de$ against the Young's modulus of the fibres, E_y and it can be seen that $d\Delta\nu/de$ is approximately proportional to E_y. The majority of the experimental points (with the exception of A7 and B7) lie close to or on a straight line which extrapolates near to the origin. This type of behaviour was found before for a series of aromatic polyamide fibres [4] where it was shown that the behaviour was consistent with the theory of Northolt and co-workers [17–19] outlined in Equations 1–3.

Fig. 10 shows that Raman microscopy essentially monitors only the molecular chain stretching and that the contribution of molecular stretching increases with fibre modulus. This can be explained as follows. It is found that $d\Delta\nu/de$ is proportional to $E_y (\approx d\sigma/de)$ and so

$$\frac{d\Delta\nu}{de_{total}} \propto E_y = \frac{d\sigma}{de_{total}} \quad (5)$$

and hence

$$d\Delta\nu \propto d\sigma \quad (6)$$

i.e. the change in Raman band position is proportional to the stress. For the stretching process, Equations 1 and 2 imply that

$$e_{stretch} = \frac{\sigma}{E_c} \quad (7)$$

then it follows that because E_c is a constant

$$d\Delta\nu \propto de_{stretch} \quad (8)$$

This shows clearly that the shift in the peak position in the Raman spectrum is related directly to chain stretching and not to crystal rotation.

Fibres A7 and B7, which have a large difference in molecular orientation (Table I), fall significantly above the $d\Delta\nu/de$ versus E_y relationship defined by the other fibres (Fig. 10). Optical absorption measurements from thin films of aromatic polyamides [32] have shown that the optical skin depth of visible light is of the order of only 1–2 μm. This is the order of the thickness of the skin regions of the fibres (Fig. 4) and means that the Raman signal using the He–Ne laser comes essentially from the skin regions of the fibres. For most of the fibres this is of no consequence because there is not a large difference between skin and core structure. However, for fibres A7 and B7 the skin regions have a significantly higher level of orientation than the core and so the measured values of $d\Delta\nu/de$ for these two fibres correspond to significantly higher values of E_y than are measured for the whole fibre. Moreover, the Raman technique can be used to estimate the values of E_y for the skin of the fibres as about 125 GPa for the skin of A7 and 115 GPa for B7. These values are similar to values of E_y for uniform fibres with similar overall values of 2θ. The higher modulus skin regions of A7 and B7 will be subjected to higher stresses than the cores (assuming a uniform strain situation) when the fibres are deformed and so will undergo premature failure at relatively low strain as described in Section 4.2.

5. Conclusions

There is an intimate relationship between the structure and mechanical properties of aramid fibres. Tensile deformation takes place by a combination of chain stretching and crystal rotation. The fibre tensile modulus is controlled by the initial degree of overall orientation plus the additional orientation which occurs as a result of crystal rotation. Transmission electron microscopy has enabled a detailed study of the variation in molecular orientation within a particular fibre and has shown that significant differences sometimes occur between the skin and core regions. The existence and magnitude of these skin/core differences is believed to be a result of the different manufacturing conditions.

Raman microscopy is useful to measure molecular deformation in aramid fibres and shifts in Raman band position are directly related to the molecular stretching process. Moreover, if a He–Ne laser is used, the deformations in the skin region can be selectively monitored and the mechanical properties of the skin regions estimated. The fracture strength of the fibres is controlled principally by the overall molecular orientation and differences in orientation between the skin and core have a significant impact upon fibre properties. Fibres with high skin/core orientation difference had lower strength than would be expected based on their overall orientation.

The results of this present study give a unique insight into the relationship between structure and properties in aramid fibres at a level never previously obtained and they should enable further advances to be made in the preparation of aramid fibres with even more impressive mechanical properties.

Acknowledgements

This work was supported at UMIST by research grants from the SERC and E.I. Du Pont de Nemours and Co. Inc.

References

1. J. R. SCHAEFGEN, in "Strength and Stiffness of Polymers", edited by A. E. Zachariades and R. S. Porter (Marcel Dekker, New York) 339 pp.
2. H. H. YANG, "Aromatic High-Strength Fibres" (Wiley, New York, 1989).
3. M.G. DOBB and R. M. ROBSON, *J. Mater. Sci.* **25** (1990) 459.
4. S. VAN DER ZWAGG, M. G. NORTHOLT, R. J. YOUNG, I. M. ROBINSON, C. GALIOTIS and D. N. BATCHELDER, *Polym. Commun.* **28** (1987) 276.
5. R. J. YOUNG, D. LU. and R. J. DAY, *Polym. Int.* **24** (1991) 71.
6. K. PRASAD and D. T. GRUBB, *J. Polym. Sci. Polym. Phys. Ed.* **27** (1989) 381.
7. R. J. DAY, I. M. ROBINSON, M. ZAKIKHANI and R. J. YOUNG, *Polymer* **28** (1987) 1833.
8. R. J. YOUNG, R. J. DAY and M. ZAKIKHANI, *J. Mater. Sci.* **25** (1990) 127.
9. R. J. YOUNG and P. P. ANG, *Polymer*, **31** (1990) 47.
10. I. M. ROBINSON, M. ZAKIKHANI, R. J. DAY, R. J. YOUNG and C. GALIOTIS, *J. Mater. Sci. Lett.* **6** (1987) 1212.
11. L. J. FINA, D. I. BOWER and I. M. WARD, *Polymer* **29** (1988) 2146.
12. W. F. KNOFF, *J. Mater. Sci.* **22** (1987) 1024.
13. L.-S. LI, L. F. ALLARD and W. C. BIGELOW, *J. Macromol. Sci. Phys.* **B22** (1983) 269.
14. E. G. CHATZI, M. W. URBAN and J. L. KOENIG, *Makromol. Chem. Makromol. Symp.* **5** (1986) 99.
15. H. H. YANG, M. P. CHOUINARD and W. J. LINGG, *J. Appl. Polym. Sci.* **34** (1987) 1399.
16. A. M. TIEFENTHALER and M. W. URBAN, *Appl. Spect.* **42** (1988) 163.
17. M. G. NORTHOLT and J. J. VAN AARTSEN, *J. Polym. Sci. Polym. Symp.* **58** (1977) 283.
18. M. G. NORTHOLT, *Polymer* **21** (1980) 1199.
19. M. G. NORTHOLT, and R. VAN DER HOUT, *ibid.* **26** (1985) 310.
20. S. R. ALLEN and E. J. ROCHE, *ibid.* **30** (1990) 996.
21. M. G. NORTHOLT and D. J. SIKKEMA, *Advances in Polymer Science* **98** (1990) 119.
22. R. J. GAYMANS, J. TIJSSEN, S. HARKEMA and A. BANTJES, *Polymer* **17** (1976) 517.
23. R. BARTON, *J. Macromol. Sci.* **B24** (1985) 119.
24. G. S. FIELDING-RUSSELL, *Tex. Res. J.* **41** (1971) 861.
25. K. TASHIRO, M. KOBAYASHI and H. TADOKORO, *Macromolecules* **10** (1977) 413.
26. H. KOOIJMAN, L. M. J. KROON-BATENBURG and M. G. NORTHOLT, to be published.
27. W. F. KNOFF, *J. Mater. Sci. Lett.* **6** (1987) 1392.
28. A. KELLY and N. W. MACMILLAN, "Strong Solids", 3rd Edn. (Oxford University Press, Oxford, 1986).
29. J. W. S. HEARLE, P. GROSBERG and S. BACKER, "Structural Mechanics of Fibres, Yarns and Fabrics" (Wiley-Interscience, New York, 1969) p. 213.
30. G. S. HOLISTER and C. THOMAS, "Fibre-reinforced Materials" (Elsevier, London, 1966) p. 213.
31. P. SMITH and Y. TERMONIA, *Polymer Commun.* **30** (1989) 66.
32. D. LU and R. J. YOUNG, unpublished data (1991).

Received 17 December 1991
and accepted 23 January 1992